Radiotherapy and Oncology 159 (2021) 126–135

Contents lists available at ScienceDirect

Radiotherapy and Oncology

journal homepage: www.thegreenjournal.com

Original Article

Comprehensive analysis of radiosensitivity in head and neck squamous cell carcinoma

Guangqi Li [a,2], Yuanjun Jiang [b], Guang Li [a,*,1], Qiao Qiao [a,*,1]

[a] Department of Radiation Oncology; and [b] Department of Urology, The First Hospital of China Medical University, Shenyang, China

ARTICLE INFO

Article history:
Received 20 October 2020
Received in revised form 9 March 2021
Accepted 9 March 2021
Available online 26 March 2021

Keywords:
Radioresistance
Single cell sequencing
Deconvolution
Immune checkpoint blockade
TCGA

ABSTRACT

Background: Radioresistance is a major barrier to the successful treatment of head and neck squamous cell carcinoma (HNSCC).

Methods: We took advantage of different types of data, including single-cell sequencing data, bulk tissue sequencing data and deconvolution data, to conduct a comprehensive analysis of HNSCC radiosensitivity at the cellular, patient, and cell type levels. Single-cell transcriptomes for 1388 primary cancer cells from a previous study were analysed. The TCGA HNSCC dataset including 499 primary HNSCC samples with RNA-seq data, DNA methylation data and clinical information were used for bulk tissue sequencing analyses and deconvolution.

Results: We found that radiosensitivity clustering of HNSCC cells was highly consistent with molecular typing, where cancer cells of the atypical subtype exhibited a higher sensitivity than those of the classical and basal subtypes. The common radioresistant gene modules of the classical and basal subtypes were mainly associated with cell division and cell cycle regulation; the classical subtype specific radioresistant module was mainly associated with metabolic pathways; and the basal radioresistant subtype specific modules included two epithelial differentiation-related modules and a module mainly associated with endoplasmic reticulum, apoptosis and focal adhesion. We developed a radioresistance score using genes that affect both the cancer cell response to radiation and the patient response to radiotherapy. An enhanced cancer-immune interaction through the PD1-PDL1/PDL2 and TIM3-Galectin9 pathways was observed in radioresistant tumours, with foldchange = 2.88 (PD1), 1.44 (PDL1), 3.22 (PDL2), 1.47 (TIM3), 1.88 (Galectin9) respectively and FDR < 0.001. Transcriptional activities related to the hypoxia response, p53 pathway, NF-kappa-B pathway and inflammatory response were abnormally activated in the radioresistant tumours (FDR < 0.05).

Conclusions: This study comprehensively discussed the radioresistance of HNSCC, identified a group of HNSCCs that were likely to benefit from combined radiotherapy and immune checkpoint blockade, and proposed new targets for the treatment of radioresistant HNSCC.

© 2021 Elsevier B.V. All rights reserved. Radiotherapy and Oncology 159 (2021) 126–135

Surgery, radiotherapy and chemoradiotherapy are the main treatments of head and neck squamous cell carcinoma (HNSCC) [1], which has become the 6th most common type of cancer worldwide [2]. Although dramatic improvements have been achieved in radiotherapy, radioresistance is still a major barrier to the successful treatment of HNSCC. The most important radiobiological factors that affect tumour responses to radiotherapy have been summarized as the "5 Rs": DNA damage Repair, cell cycle Reassortment, Repopulation, Reoxygenation and cancer cell-intrinsic Radiosensitivity [3]. Recently, reactivation of the antitumour immune response has been regarded as the 6th "R" [4], extending the concept of radiosensitivity beyond tumour cells themselves and supporting improved outcomes when radiotherapy is combined with immunotherapy.

With the development of gene sequencing technology in recent years, many gene signatures have been developed to predict tumour radiosensitivity. These signatures can be divided into two categories: signatures developed using the surviving fraction of cancer cell lines after radiation [5–7] and signatures that predict

Abbreviations: HNSCC, head and neck squamous cell carcinoma; DEGs, differentially expressed genes; WGCNA, weighted gene co-expression network analysis; PFI, progression-free interval; tr-PFI, treatment related progression-free interval; TFs, transcription factors.

* Corresponding authors at: Department of Radiation Oncology, The First Hospital of China Medical University, Shenyang 110001, Liaoning, China.

E-mail addresses: liguangqimed@hotmail.com (G. Li), qiaojiang120@126.com (G. Li), braveheart8063@outlook.com (Q. Qiao).

[1] These authors contributed equally to this work.

[2] Author for statistical analyses.

https://doi.org/10.1016/j.radonc.2021.03.017
0167-8140/© 2021 Elsevier B.V. All rights reserved.

patient progression after radiotherapy [8,9]. The former reflects cancer cell-intrinsic radiosensitivity; however, these signatures do not take into account the effects of nonmalignant cells in the tumour microenvironment, especially the role of antitumour immunity. The latter is dedicated to predicting the clinical efficacy of radiotherapy; however, these signatures cannot be used for cell-level research, and are difficult to reveal the mechanism based on radiobiology. Torres-Roca and his team developed a radiation sensitivity index (RSI) based on the cellular radiation survival curve [6], which was then validated in multiple clinical cohorts [10–16]. Based on the RSI and the linear quadratic model they developed the genomic-adjusted radiation dose (GARD) to guide clinical use of radiotherapy [17], which has been proposed as the first opportunity for a genomically driven personalized approach in radiation oncology [18,19]. In addition to the classic biological mechanisms mentioned above, gene sequencing has further revealed the regulatory function of non-coding RNA on radiation sensitivity [20-24]. Its high-throughput feature facilitates the study of radiosensitivity mechanisms.

Traditional bulk tissue sequencing considers a tumour to be homogeneous and always reflects mixed signals. Single-cell RNA sequencing (scRNA-seq) technologies, which have been rapidly developed in recent years, have revealed complex cell populations and are powerful tools for studying intratumour heterogeneity. Although scRNA-seq enables the independent sequencing of tens of thousands of cells, the number of tumours analysed is usually limited [25,26], even if all the existing data sets are merged. Many analyses at the cell type level that require sufficient tumour numbers are difficult to perform. Deconvolution technology for bulk tissue sequencing fills this gap [27–30]; this approach calculates the cell type composition of a sequenced bulk tissue sample and estimates the expression profiles for the constituent cell types. In this study, we used scRNA-seq data to explore the intercell heterogeneity of HNSCC cell responses to radiation and deconvoluted TCGA bulk tissue data to explore the different mechanisms of cancer-immune crosstalk and transcription factors (TFs) activation between radiosensitive and radioresistant tumours. The cell response to radiation and patient response to radiotherapy were distinguished and linked in this article.

Methods and materials

Datasets

The scRNA-seq data and the non-negative matrix factorization (NMF) program scores were previously published [31]. Single-cell transcriptomes for 5902 cells from 18 HNSCC patients with both more than 2000 detected genes and an average housekeeping expression level (E) above 2.5 passed initial quality controls [31]. Since not all the 18 tumours were characterized deeply enough, they selected 10 tumours with largest numbers of malignant cells for analysis. To keep our results comparable, a total of 1388 primary cancer cells from the 10 patients were selected in this study. According to Puram et al., NMF was used to reveal coherent sets of genes co-expressed by subsets of cancer cells. The NMF approach determined 6 gene signatures that vary among malignant cells of one tumour. Therefore, 60 signatures were extracted after applying the approach to each of the 10 tumours. Then, hierarchical clustering was used to distil these 60 signatures into 6 meta-signatures (called programs) reflecting common patterns of intra-tumoral heterogeneity.

The TCGA HNSCC bulk tissue sequencing data, including the normalized RNA-seq data, DNA methylation data and somatic copy-number data, were downloaded from https://portal.gdc.cancer.gov/. The phenotype data of the TCGA cohort were downloaded from UCSC Xena (http://xena.ucsc.edu/). A total of 499 primary HNSCC samples with RNA-seq data, DNA methylation data and clinical information were analysed in this study. The somatic copy-number data of 299 samples was used to calculate ABSOLUTE score for validation. The 303 reference methylation profiles of the known cell types used for deconvolution were gathered from the Gene Expression Omnibus (GEO, https://www.ncbi.nlm.nih.gov/geo/).

Radiosensitivity signatures

A 31-gene signature [5] was used for radiosensitivity clustering of single HNSCC cells. The signature was developed using multi-platform microarrays of NCI-60 cell lines, with the survival fraction at 2 Gy (SF2) as a measure of radiosensitivity. Using significant analysis of microarrays (SAM), the author identified 31 genes as common to all the microarray platforms. Therefore, the 31-gene signature was defined as a common radiosensitivity signature, which has been validated to predict radiotherapy responses in multiple cancer types including the TCGA HNSCC [32].

The radiation sensitivity index (RSI) [6] was used to compare the radiosensitivity scores of the three clusters identified by the 31-gene clustering. This index was primarily developed using 48 human cancer cell lines as a rank-based linear regression algorithm to predict an intrinsic radiosensitivity, which was then validated in multiple clinical cohorts [10–16].

Comparative analysis of the weighted gene coexpression networks

The differentially expressed genes (DEGs) between the radiosensitive cells and radioresistant cells (|foldchange|>1.5, FDR < 0.05) were used to independently construct weighted coexpression networks in the classical and basal subtypes using weighted gene co-expression network analysis (WGCNA) [33]. The networks were constructed with networkType = signed. The soft power thresholds used to construct the networks were selected to simultaneously satisfy scale-free topology (R^2 > 0.85) and relatively higher connectivity. The modules were identified and then related to the selected traits through eigengene-based Pearson correlation analysis. This process was repeated using the common genes in the two networks to perform the convergence analysis of the modules from the different subtypes, which was designed to explore the connectivity and differences of the two networks based on co-expression modules.

Radiotherapy-related progression-free interval in the TCGA dataset

We referred to the method of [34] to define the treatment related progression-free interval (tr-PFI): The time from the start of radiation to "progression of the disease, locoregional recurrence, distant metastasis, new primary tumor, or death with tumor" [35] was defined as "radiotherapy-related progression-free interval (rr-PFI)". If the patient did not experience these ending events after radiation, rr-PFI was defined as the time from the start of radiotherapy to the last follow-up.

Deconvolution of the TCGA dataset

The deconvolution used both the DNA methylation profiles and RNA-seq profiles. The Edec package [27] was used for the deconvolution. In Edec-stage 0, we selected a total of 303 450 k methylation profiles as references, which were classified into cancer, stromal and immune cell lines. After removing the loci with missing values and that were known to contain overlapping common single nucleotide polymorphisms [27], 400 loci with the greatest differences across the cell types (p < 1E-10) were selected, and these loci were proven to accurately differentiate the cell types

(Fig. 5A). These loci were used in Edec-stage 1 to deconvolute the methylation profiles of the TCGA dataset. We selected 3 as the cell type number to obtain by running the estimate-stability function. The correlation matrix plot showing the 3 estimated cell types of the TCGA dataset corresponded to one cancer cell type, one stromal cell type and one immune cell type. Edec-stage 2 estimated the cell type gene expression profiles through a constrained least squares fit using the cell proportions estimated in stage 1.

Tumour inflammation score (TIS) calculation

Before the calculation of the TIS, we renormalized the FPKM data using 11 housekeeping genes (expression of gene a = log2 ($FPKM_a$ + 1) − arithmetic mean of log2($FPKM_{housekeeping}$ + 1)). The TIS was computed as the weighted sum of the housekeeping gene-based normalized expression of the 18 genes [36].

Statistical analysis

Fig. 1 briefly summarizes the analysis procedure used in this article. All the statistical analyses were performed using R software (v3.6.3). The "ConsensusClusterPlus" package [37] was used for cell clustering using the k-means method. The "Seurat" package was used to perform the dimension reduction of the whole scRNA-seq data. The Wilcox test, the "edgeR" package and the t/t' test were used for DEG identification in the scRNA-seq data, bulk tissue sequencing data and deconvoluted data, respectively. Cox regression and survival analysis were performed using the "survival" package. The immune cell proportion was estimated using CibersortX. The T cell dysfunction score was calculated using Tumor Immune Dysfunction and Exclusion (TIDE) [38]. The gene set enrichment analyses were performed using the Database for Annotation, Visualization and Integrated Discovery (DAVID 6.8 https://david.ncifcrf.gov/). Cytoscape software (v3.7.1) was used for visualization of the TF regulation network.

Results

To study the heterogeneity of sensitivity to radiation in HNSCC cells, we selected 10 samples with sufficient cancer cells from a scRNA-seq data set [31]; these samples included 1388 primary cancer cells that passed quality control. A 31-gene signature that was developed using the survival fraction at 2 Gy (SF2) of NCI-60 cell lines was selected to measure the sensitivity of a cancer cell to radiation [5]. The signature was developed using multiplatform data and has been validated to predict radiotherapy responses in the TCGA HNSCC [32]. Consensus clustering was performed with the 1388 cancer cells based on the 31 radiosensitivity-related genes. According to the cumulative distribution function (CDF) plot (Fig. 2A), we selected $k = 3$ to perform the clustering, which divided the cancer cells into three clusters with different patterns of radiosensitivity (Fig. 2B) [37]. The consensus matrix showed high consensus value among cells within the same cluster and low consensus value between cells belonging to different clusters (Fig. 2B). These three clusters represented three distinct expression patterns based on the 31 radiosensitivity genes. To verify the clusters and identify the sensitive and resistant clusters, we used another radiotherapy sensitivity indicator, RSI [6], which is a linear model consisting of ten gene expression levels. As shown in Fig. 2C, the cancer cells in cluster 1 showed a significantly lower RSI than the cancer cells in the other two clusters ($P < 0.01$), which indicates that the cancer cells in cluster 1 exhibit a significantly higher sensitivity to radiation. The cells in cluster 2 showed a higher mean RSI than the cells in cluster 3; however, the difference was not significant.

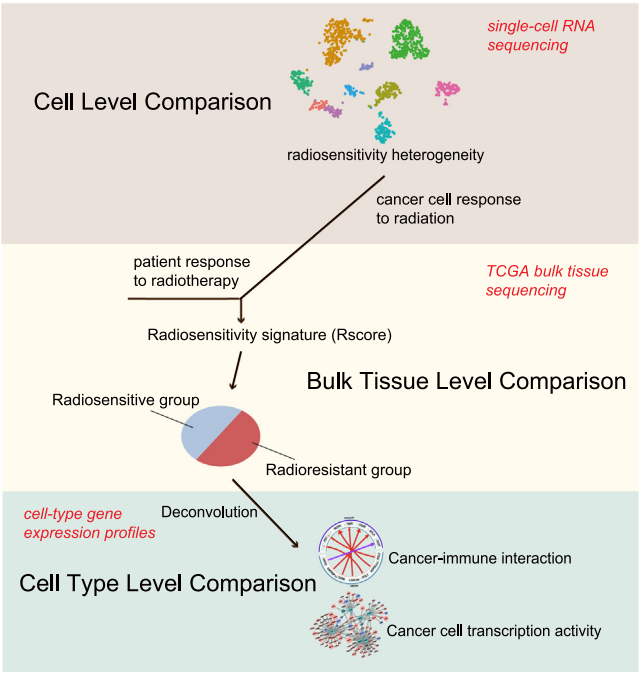

Fig. 1. A brief summary of the research procedure. This study started with single-cell RNA sequencing data to explore the heterogeneity in the response to radiation in cancer cells. Using genes that affect both the cancer cell response to radiation and the patient response to radiotherapy, we developed a radiosensitivity score to divide TCGA HNSCC into two groups. The bulk tissue sequencing data were then deconvoluted to obtain cell type gene expression profiles. Cancer-immune interaction and transcription activation analyses in cancer cells were performed based on the deconvoluted profiles.

We then used the "Seurat" package to perform the dimension reduction of the whole scRNA-seq data and reclustered the 1388 primary cells. Consistent with the clustering results in [31] (which included the cancer cells from lymph nodes), the cancer cells clustered according to their sample origin (Fig. 2D), which was mainly caused by CNVs that vary between tumours [31]. The "Seurat" algorithm selects genes with the highest variability among cells to perform the reduction. When we perform the algorithm based on the entire transcriptome, the differentially expressed genes caused by CNV account for most of the genes with highest variability. Therefore, clustering pattern mainly reflected the differences among individuals. However, when we annotated the molecular subtype (estimated from the TCGA subtype signature mapped to single cell) and radiosensitivity clustering information of these cells, we were surprised to find that the two patterns were highly consistent (Fig. 2E). Since the radiosensitivity grouping was obtained by unsupervised clustering, this result suggested that the sensitivity of HNSCC cells to radiation might be mainly affected by molecular subtypes. Compared with the atypical subtype, the classical and basal subtypes showed significantly higher resistance to radiation. The radiotherapy-related progression-free survival (rr-PFI, see METHODS) of the patients with atypical tumours in the TCGA HNSCC was significantly longer than that of the patients with tumours of other molecular subtypes (Supplementary Figure A). The RSI scores of atypical TCGA tumours were significantly lower than tumours in other subtypes (Supplementary Figure B). This finding confirms the commonality of patient responses to radiotherapy and tumour cell responses to radiation. However, there are only 34 PFI events in this analysis, and the PFI events may include distant metastases or deaths unrelated to the efficacy of adjuvant radiotherapy, which limits the significance of this result.

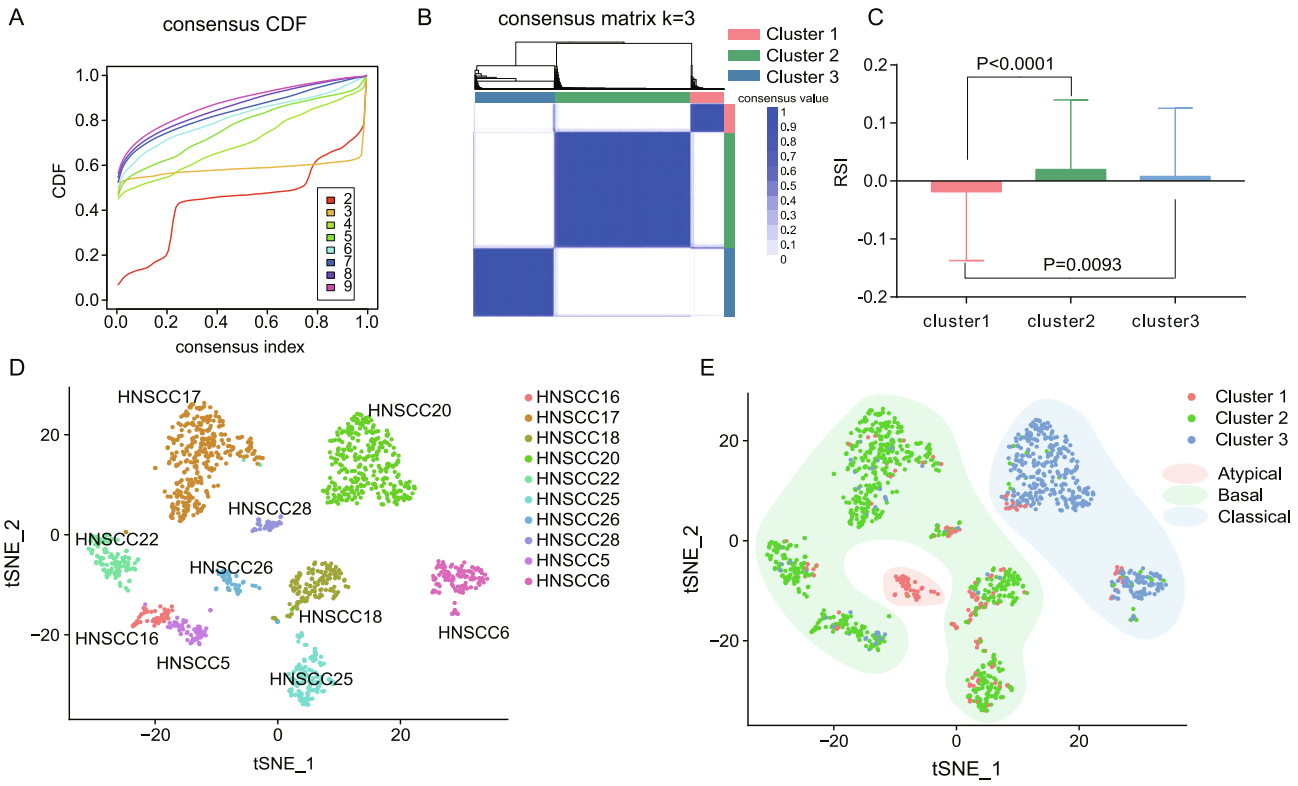

Fig. 2. Radiosensitivity clustering of single HNSCC cells. A, Cumulative distribution function (CDF) plot of the clustering to identify the proper number of clusters. The different colours represent the different number of clusters. B, Consensus clustering matrix of the tumour cells based on the 31-gene signature. The 1388 single cells were set as both rows and columns, where consensus values range from 0 (never clustered together) to 1 (always clustered together) marked by white to dark blue. The consensus values were calculated by ConsensusClusterPlus based on euclidean distance, and cells were clustered through k-means clustering algorithm. The three clusters represented three distinct expression patterns based on the 31 radiosensitivity genes. C, Radiosensitivity index (RSI) of the three clusters displayed with mean value and standard deviation (SD). D, Dimension reduction of the whole scRNA-seq data and reclustering of the 1388 primary cancer cells using the "Seurat" package. The name of the 10 patients is consistent with the original data set. E, Annotation of the TCGA molecular subtypes and radiosensitivity clusters.

According to [31], the malignant cells in HNSCC could be divided into three subtypes (basal, classical and atypical), while the previously identified mesenchymal subtype [39] in bulk samples was actually a stromal-enriched basal subtype. The first step clustering based on the 31 genes only identified the most significant factor affecting the radiosensitivity. Since the atypical subtype, which was identified as a radiosensitive subtype, only accounts for 24% of HNSCC, we continued to study the resistance mechanisms of the classical and basal subtypes using the sc-RNA transcriptome. Using the consensus clustering based on the 31 genes, we classified the 444 classical cells (from 2 patients) into a relatively sensitive cluster (138 cells) and a relatively resistant cluster (306 cells); the 887 basal cells (from 6 patients) were also divided into a relatively sensitive cluster (291 cells) and a relatively resistant cluster (596 cells) (Supplementary Figure C-D). We used DEGs (|foldchange|>1.5, FDR < 0.05) between the relatively sensitive and relatively resistant clusters to construct weighted gene coexpression networks within the two subtypes of cells, respectively. Using WGCNA with parameters described in METHOD, we constructed two scale-free networks and identified 4 gene coexpression modules (C1-C4) in the classical subtype network and 5 gene co-expression modules (B1-B5) in the basal subtype network. Each informative module included a group of coexpressed genes from the corresponding topological network. The 4 TCGA molecular subtype signature scores mapped to single cells and the 6 program scores identified using nonnegative matrix factorization (NMF) [31] were selected as traits (the horizontal axis of Fig. 3 A, B, F, G) to be related to the modules identified in our coexpression networks. The 4 subtype signatures helped us to verify the modules that were specific to the classical or basal subtypes; the 6 NMF programs were generated from the original research and represented the most prominent expression patterns in the malignant cells of this dataset. Coexpression modules were identified in each network (Supplementary Figure E-F) and were related to the 10 trait signatures (Fig. 3A-B). The correlation to the traits was based on the eigengenes which represent the main characters of the module. According to the correlation pattern to the 10 signatures, we noticed that some modules in the two networks shared similar biological behaviours, such as C3/C4 with B1 (cell cycle related) and C1 with B3 (negative related to epithelial differentiation). To compare the two networks, we used the 896 common radiosensitivity DEGs shared by the classical and basal subtypes to construct two coexpression subnetworks in the two subtypes. The two subnetworks were constructed using the same parameters to perform the convergence analysis of the modules from the different subnetworks. As shown in Fig. 3C-D, the two subnetworks were comparable in terms of both expression and connectivity. Obviously, connectivityis better than gene expression to distinguish the genes. Therefore, the convergence analysis was based on the connectivity. The module preservation plot (Fig. 3E) showed that the cell cycle-related modules (coC2 and coB3/coB4) were highly conserved in the two subnetworks; modules coC1 and coB1 (upregulated in the radiosensitive cells), which were negatively related to malignant signatures (Fig. 3F-G), were also conserved in the two subnetworks; and coC3 (mapped to C2) and coB2 (mapped to B2) were specific to their subtype signatures. These modules represented the common and specific gene patterns related to radiosensitivity in the two subtypes. Furthermore, the

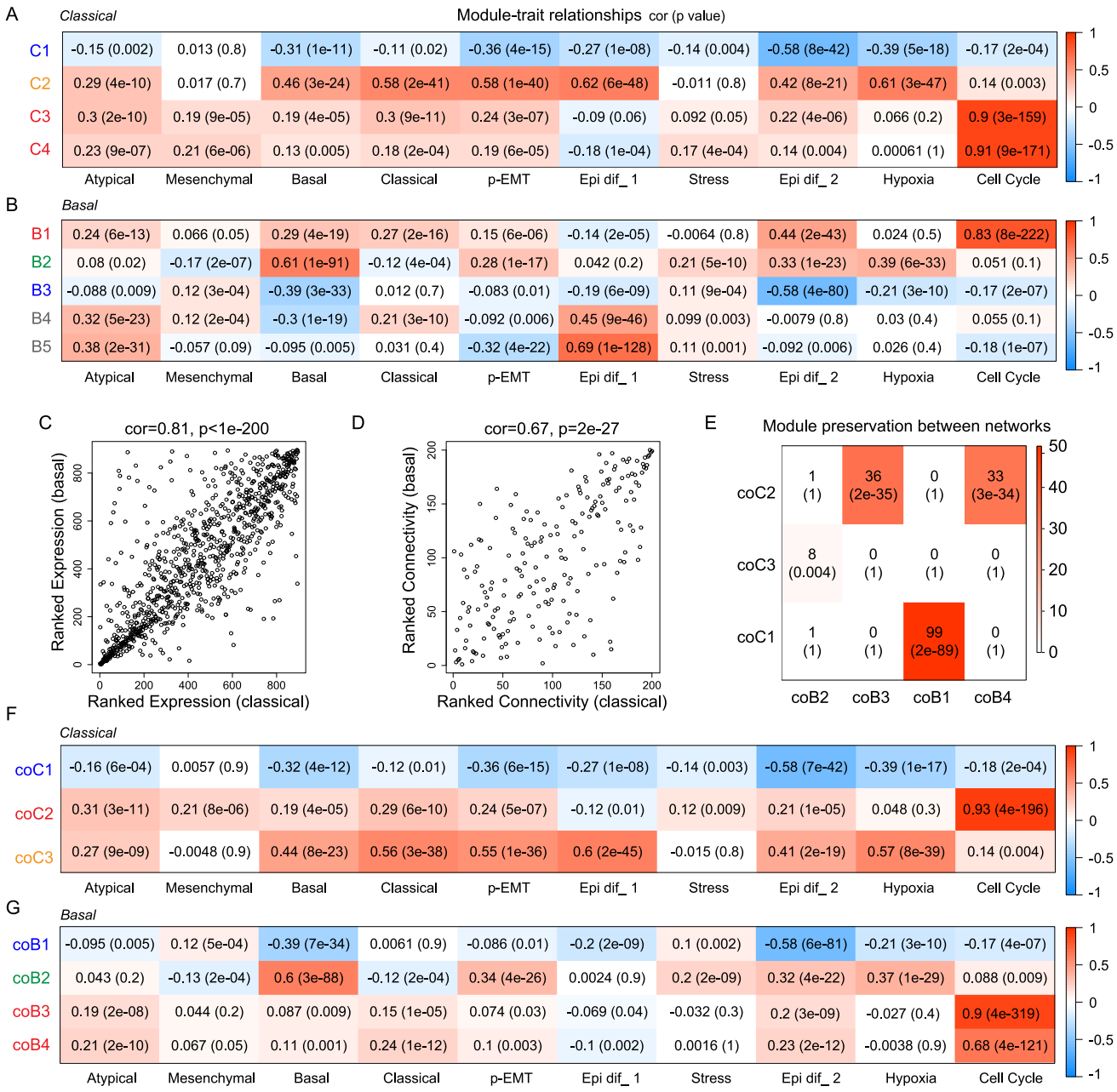

Fig. 3. Comparative network analysis of the classical and basal subtypes of the cancer cells. A-B, Correlation of the informative coexpression modules and signature traits in the classical network and the basal network. The numbers represent correlation coefficient with p-value in brackets. Each gene module was related to each selected trait through eigengene-based Pearson correlation analysis. Eigengenes are member genes of a module with high connectivity in the network and represent the main biology character of the module. C, Correlation of the ranked gene expression in the classical and basal subnetworks. D, Correlation of the ranked gene connectivity in the classical and basal subnetworks. E, Module preservation analysis between the two subnetworks. The numbers represent overlapping genes in the two modules with correlation p-value in brackets. F, Correlation of the informative coexpression modules and signature traits in the classical subnetwork. G, Correlation of the informative coexpression modules and signature traits in the basal subnetwork.

colour of the module label indicates the module mapping between the network and its subnetwork. Obviously, B4 and B5 were not reproduced in the subnetwork, which means that these two epithelial differentiation-related modules only appeared in the basal subtype network and did not account for the radioresistance of the classical subtype. We further performed GO and KEGG enrichment analyses on the hub genes (top 50% connectivity) of each informative module (Supplementary table 1). Similar modules of the two subtypes were selected from the subnetworks (coC1 ∩ coB1 and coC2∩(coB3 ∪ coB4)), while the modules specific to each subtype were selected from the complete networks (C2, B2, B4 and B5). In general, the common resistant modules were mainly associated with cell division and cell cycle regulation; the classical subtype specific module was mainly associated with metabolic pathways; the basal subtype specific modules included two epithelial differentiation-related modules and a module mainly associated with endoplasmic reticulum, apoptosis and focal adhesion. Interestingly, the hub genes of C2, B2, B4 and B5 all exhibited an enrichment in extracellular exosomes, which suggested that radioresistant HNSCC cells might exhibited increased exosome synthesis.

The 896 common genes in the two networks represented the common mechanisms of the HNSCC response to radiation at the cancer cell level. However, the interpretation of radiosensitivity

in the clinic ultimately focuses on progression-free interval (PFI) after receiving radiotherapy. Therefore, we examined the effect of these common genes on the rr-PFI of 94 TCGA HNSCC patients who received radiotherapy without chemotherapy after surgery. Fourteen genes showed a significant effect on rr-PFI in a univariate Cox analysis. A Cox proportional hazards model using these 14 genes was validated to independently and accurately distinguish the radiosensitive and radioresistant tumours in the TCGA HNSCC (Fig. 4). The risk score (Rscore) was calculated as a linear combination of the regression model coefficients (β) multiplied by the mRNA expression level (Supplementary table 2). To confirm that Rscore was indeed radiotherapy-related, we further examined the effect of Rscore on the prognosis of 148 HNSCC without radiotherapy, and found that neither PFI nor OS was affected by Rscore (Supplementary Figure G-H). At the same time, we found that in samples with radiotherapy alone, Rscore also significantly affected OS, with a lower significance and lower AUC than affecting rr-PFI (Supplementary Figure I-J). Using the median Rscore, we divided all of the 499 TCGA primary HNSCC samples into two groups (radiosensitive, RS; radioresistant, RR). The clinical characteristics of the patients in the two groups are shown in Supplementary table 3. In order to improve the reliability of the grouping on biological meaning, we then compared the different radiosensitivity-related biological signatures between the two groups using single sample gene set enrichment analyses (ssGSEA). Compared to the samples in the RS group, the samples in the RR group exhibited higher enrichment in cell cycle regulation, DNA damage repair, the p53 pathway and epithelial-mesenchymal transition and lower enrichment in oxidative phosphorylation and apoptotic signalling to DNA damage (FDR < 0.05, Supplementary table 4), which are consistent with our existing knowledge of radiosensitivity.

The malignant cell clustering and network analyses were based on the 31-gene signature, which was generated based on the survival fraction of a pure cell line after radiation at 2 Gy (SF2) *in vitro*. However, the survival of *in vivo* cancer cells after radiation is also influenced by nonmalignant cells in the tumour microenvironment, especially by antitumour immunity. The 31-gene signature could not include this influence. Since we successfully divided the TCGA primary HNSCC samples into RR and RS groups using the Rscore based on genes that affect both cancer cell radiosensitivity and patient rr-PFI, we then used a deconvolution method (Edec [27]) to obtain the cell type transcription profiles of the two groups of samples to explore the different cancer-immune interactions between the RS and RR tumours. The deconvolution was performed in 2 steps. In the first step, the proportions of cancer cells, stromal cells and immune cells in each bulk sample were estimated using constrained matrix factorization of the methylation profiles (Fig. 5B), and 303 GEO profiles of known cell types (Supplementary table 5) were used as references (Fig. 5A). In the second step, the gene expression profile of each cell type was estimated through a constrained least squares fit using the cell proportions estimated in step 1. To verify the deconvolution results, we compared the proportions of the cancer cell types obtained in the first step with the cancer purity calculated by the ABSOLUTE method [40] using somatic copy-number data. The cancer purity estimated by the two methods showed a high correlation (Cor = 0.81, $p < 0.0001$, Fig. 5C).

The "iTALK" program [41] was used to compare the cancer-immune interactions between the RR and RS tumours using the deconvoluted gene expression profiles of the different cell types. The built-in ligand-receptor database in "iTALK", which contains 2648 known interacting ligand-receptor pairs, was used. All the increased or decreased cancer-immune interactions in the RR tumours compared with those in the RS tumours are listed in Supplementary table 6. Gene pairs associated with immune checkpoints, which may play an important role in the resistance to radiotherapy from the perspective of cancer-immune crosstalk, were visualized using Circos plots (Fig. 5D). The well-known PD1 (*PDCD1*)-PDL1 (*CD274*)/PDL2 (*PDCD1LG2*) and TIM3 (*HAVCR2*)-Galectin9 (*LGALS9*) pathways were significantly activated in the RR tumours (foldchange = 2.88(PD1), 1.44(PDL1), 3.22(PDL2), 1.47(TIM3), 1.88(Galectin9), FDR < 0.001) and are important targets in immune checkpoint blockade therapy. TIM3 and PD1 are coexpressed, which is associated with T cell exhaustion and impaired T cell function [42–44]. Co-blockade of TIM3 and PD1 is more efficient than blockade of PD1 alone in several cancer models [44–47]. A triple therapy of anti-PD-1, anti-TIM3 and focal radiation led to significant improvements in survival compared with other arms of treatment in murine gliomas [48]. This result made us to speculate that patients with RR tumours and high expression of PD1/TIM3 pathway might benefit more from combination therapy of radiation and checkpoint blockade. Furthermore, the BTLA-HVEM (*TNFRSF14*) axis also plays a critical role in T cell suppression [49], with corresponding blockers under development [50].

To verify the speculation, we identified a "Triple Group" of 101 tumours in TCGA primary HNSCC, whose PD1-PDL1/PDL2 and TIM3-Galectin9 expression were upregulated with a higher Rscore (top 50%). We tried to compare the immune microenvironment and tumour inflammatory signature (TIS) between the Triple Group and other samples to verify whether it is more likely to ben-

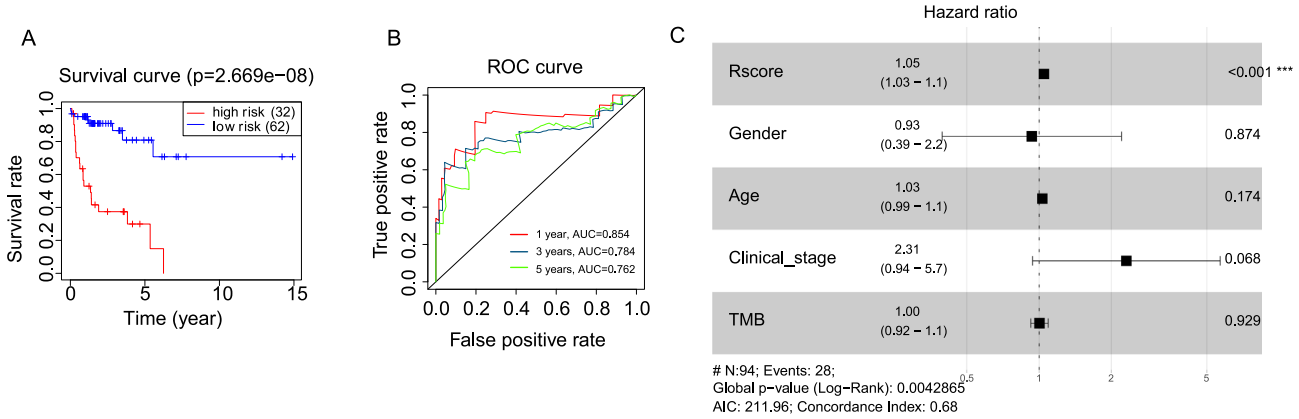

Fig. 4. Validation of the Rscore. A, The high- and low-risk groups that were identified according to the Rscore showed significantly different radiotherapy-related progression-free survival. The cut-off value was identified using the "surv_cutpoint" function of the "survminer" package. B, Receiver operating characteristic curve at 1, 3 and 5 years. C, Multivariate Cox analysis combining the Rscore and other clinical features. The results suggested that the Rscore predicted radiation-related PFI independently of these clinical features.

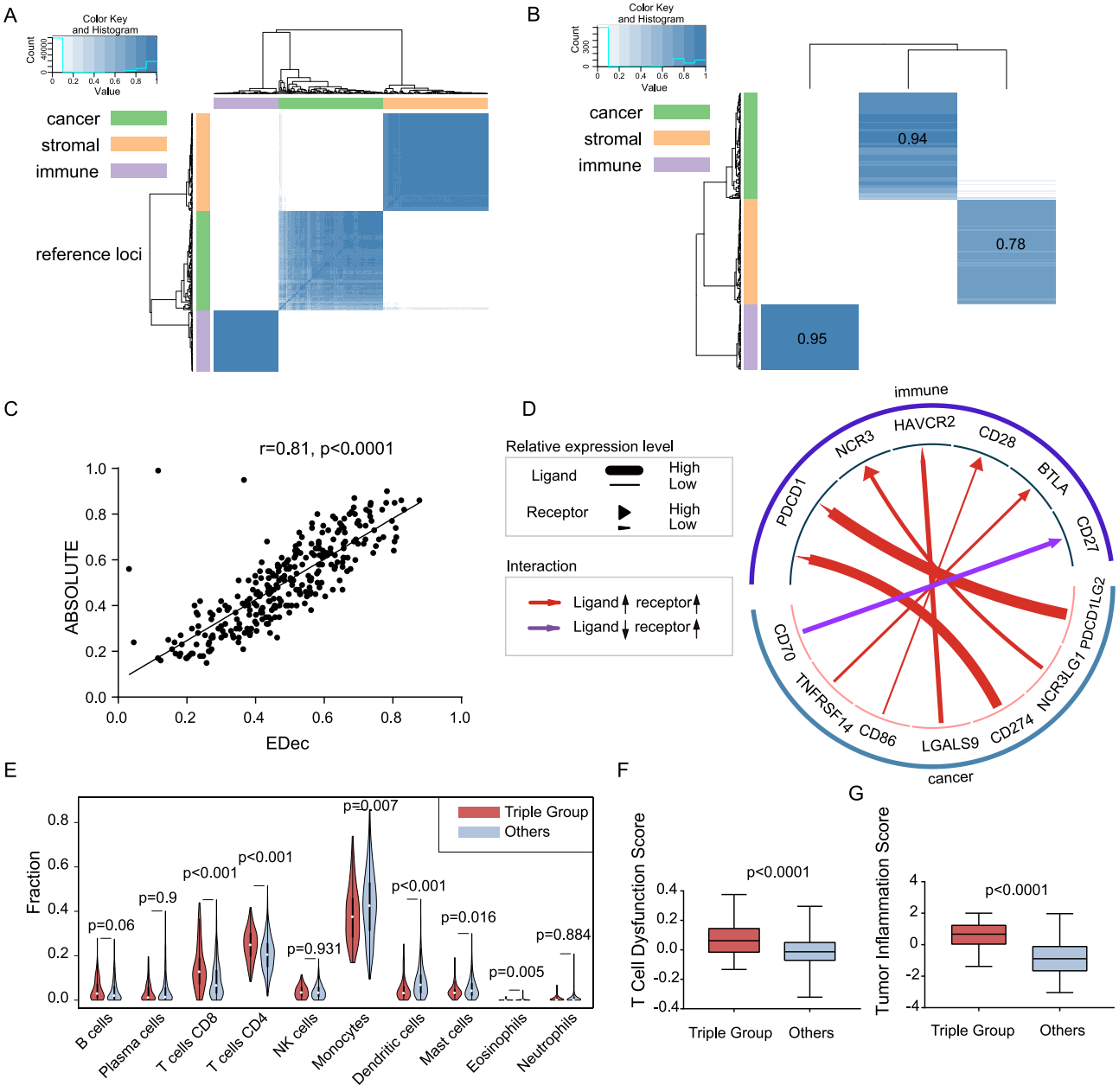

Fig. 5. Deconvolution and cell type interaction analysis of the TCGA dataset. A, Clustering heatmap of the selected reference loci. In EDec-stage 1, the algorithm selected 400 loci from the 450 k loci to distinguish the three reference types. The heatmap shows high correlation within each cell type and low correlation between cell types. B, Correlation matrix of the estimated cell types in the TCGA dataset and the reference cell types shows the 3 estimated cell types of the TCGA dataset corresponded to one cancer cell type, one stromal cell type and one immune cell type. C, Correlation of the cancer purity estimated by the ABSOLUTE method and the cancer cell proportions deconvoluted by EDec. D, Significantly changed cancer-immune checkpoint interactions in the radioresistant tumours compared with those in the radiosensitive tumours. E-G, Immune cell proportions, T cell dysfunction score and tumour inflammation score between the tumours in the Triple Group and others.

efit from combined immunotherapy. We performed CibersortX to compare the relative immune cell infiltration of the Triple Group to others. The tumours in the Triple Group showed a lower infiltration of dendritic cells (P < 0.001, Fig. 5E), which suggests a decreased antigen presentation function. The proportions of CD8 + and CD4+ T cells were significantly increased in the tumour microenvironment of the Triple Group, with a higher dysfunction score (P < 0.0001, Fig. 5F) [38]. The induction of T cell dysfunction in tumours with high infiltration of cytotoxic T cells is one of the two primary mechanisms of tumour immune evasion [38]. A previously developed tumour inflammatory signature (TIS) which has been proved to predict the benefit of immune checkpoint blockade [36,51] was significantly higher in the tumours in the Triple Group (P < 0.0001, Fig. 5G). These comparisons support our speculation that patients with RR tumours and high expression of PD1/TIM3 pathway may benefit more from combination therapy of radiation and immune checkpoint blockade. However, more direct evidence is needed to support and verify the speculation.

To further identify therapeutic targets in the cancer cells themselves, we analysed the deconvoluted gene expression profiles of the cancer cell type in the TCGA dataset. Due to the central role of TFs in tumour biology, we focused on significantly activated TFs in the RR samples compared to the RS samples. Instead of comparing the expression of the TFs themselves, the significance of a TF activation was measured by Fisher's exact test on its target genes. A total of 3144 TF-target activation relationships and 1922 TF-

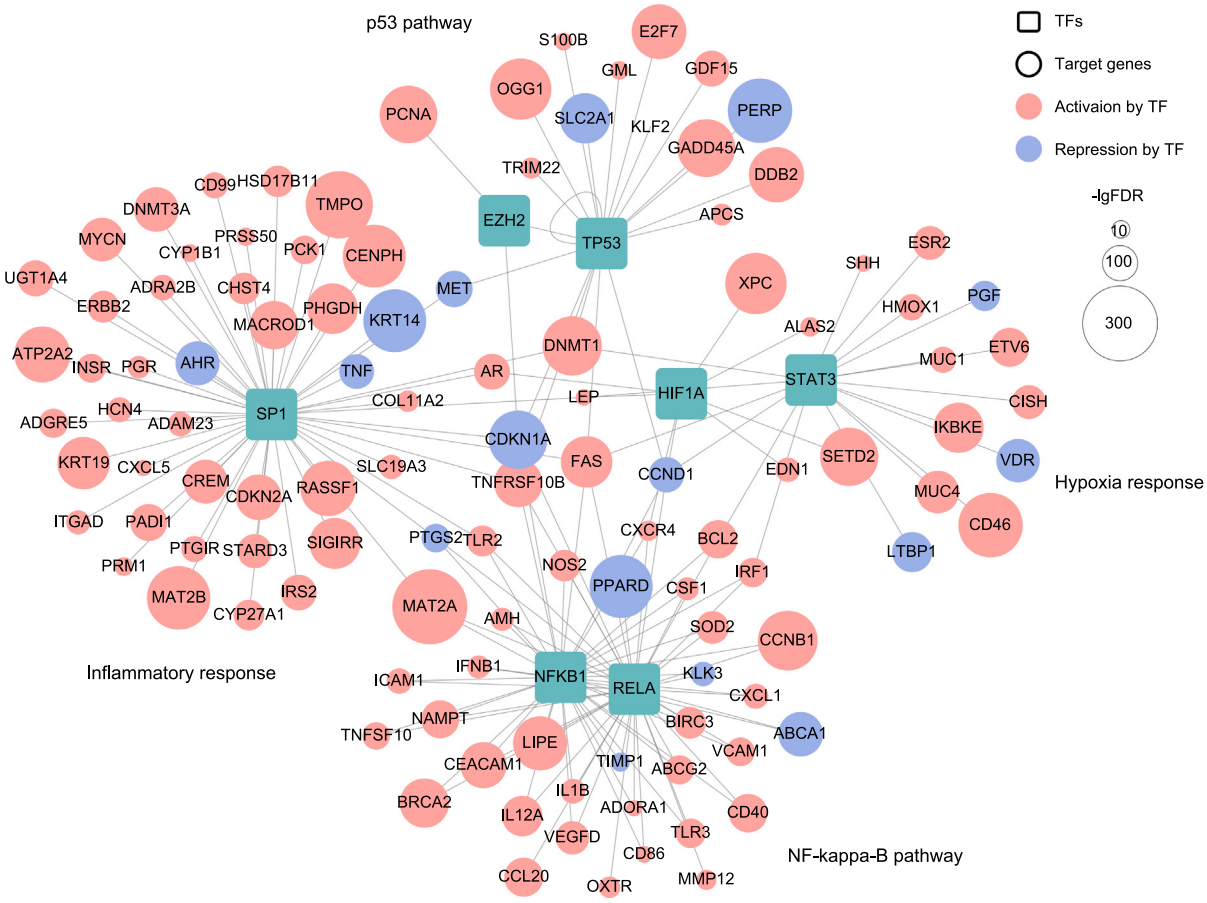

Fig. 6. Significantly activated transcription factors and their target differentially expressed genes in the radioresistant tumours compared with the radiosensitive tumours.

target repression relationships derived from published articles were downloaded from TRRUST [52]. For each TF, T_{ac} represented a collection of its target genes with activation relationships, and T_{re} represented a collection of its target genes with repression relationships. G_{all} represented the collection of all the protein-coding genes; G_{up} represented the genes that were significantly overexpressed in the RR samples compared to the RS samples; and G_{down} represented the genes that were significantly underexpressed in the RR samples compared to the RS samples. The P value of TF activation was calculated as:

$$p = \left(\frac{a+b}{a}\right)\left(\frac{c+d}{c}\right) / \left(\frac{a+b+c+d}{a+c}\right),$$

where $a = |T_{ac} \cap G_{up}| \cup |T_{re} \cap G_{down}|$ represents differentially expressed target genes, $b = |G_{up} \cup G_{down}| - a$ represents differentially expressed nontarget genes, $c = |T_{ac} \cup T_{re}| - a$ represents nondifferentially expressed target genes and $d = G_{all} - a - b - c$ represents nondifferentially expressed nontarget genes. Seven TFs (*TP53, EZH2, NFKB1, RELA, STAT3, HIF1A,* and *SP1*) with adjusted P values (FDR) less than 0.05 were considered activated in the RR samples. The TFs and their target DEGs are shown in Fig. 6. The target genes of *STAT3* and *HIF1A* were enriched in the hypoxia response; the target genes of *NFKB1* and *RELA* were associated with the NF-kappa-B pathway; the target genes of *TP53* and *EZH2* were associated with the p53 pathway; and the target genes of *SP1* were involved in various functions, including the inflammatory response.

Discussion

This article took advantage of different types of data, including bulk tissue sequencing data, single-cell sequencing data and deconvolution data, to conduct a comprehensive analysis at the patient, cell and cell type levels. The study explored the mechanism of radioresistance in HNSCC from two perspectives: the response of cancer cells to radiation and the response of tumour patients to radiotherapy. The former improves the resolution of the study to cellular level, revealing the radiosensitivity heterogeneity of different subtypes and the common and distinct mechanisms of resistance in different subtypes. The latter used large-population deconvoluted data to explore radiotherapy resistance based on cancer-immune cell interactions and TF activation. The Rscore developed in this study connected these two perspectives, using genes that affect both the cellular sensitivity and patient sensitivity to divide the TCGA HNSCC patients into groups. A previous study used the intersection of the cell line-level DEGs and the patient-level prognostic genes to construct a radiosensitivity signature [53]. The signature was computed and validated as the single sample gene set enrichment score (ssGSEA) of the 13 genes; however, the 13 genes include both sensitive and resistant genes, which should not be placed in the same gene set for enrichment.

An important finding in this study is the enhanced immune checkpoint interactions in radioresistant tumours, which provides a new theoretical basis for combination therapy of radiotherapy and immune checkpoint blockade for HNSCC. We identified a group of radioresistant HNSCC with enhanced interactions of PD1-PDL1/PDL2 and TIM3-Galectin9, and this group exhibited

weakened antigen presentation function and high dysfunctional T cell infiltration. The tumours in this group may be suitable for combination therapy with radiotherapy and immune therapy, which requires further functional experiments and clinical verification. The ongoing and planned clinical trials with the co-blockade of TIM3 and PD1/PDL1 were reviewed in [54]. Several preclinical models have reported an increased effect when radiotherapy was combined with PD-1/PD-L1 or TIM3 blockade [48,55–57]. Abnormally activated TFs in cancer cells of the RR group compared with those in the RS group reflected the effect of transcriptional activity on radiosensitivity. We innovatively explored the changed transcriptional activities from a functional perspective rather than traditional differential gene expression, making the results more reflective of biological significance. The abnormally activated TFs and their regulated DEGs were related to the hypoxia response, p53 pathway, NF-kappa-B pathway and inflammatory response. The abnormally activated transcription network could reveal candidate targets for the treatment of radioresistant HNSCC.

There are still some limitations in this study. The conclusions obtained in this study, especially the radiosensitivity mechanisms based on deconvolution, are essentially correlative observations. Functional validation is need to get rigorous causative conclusions.

Conclusions

This study distinguishes the different meanings of "radiosensitivity" and explains their mechanisms from multiple levels. These conclusions suggest the possibility that combination with immune therapy may solve the problem of radioresistance in HNSCC.

Data availability statement

All data generated and used during this study are described in the Methods or the supplementary files.

Competing interests statement

The authors declare no conflicts of interest.

Funding

This research was funded by the Key Research and Development Plan of Liaoning province (Department of Science and Technology of Liaoning Province, grant no. 2017225023).

Acknowledgements

NA.

Appendix A. Supplementary data

Supplementary data to this article can be found online at https://doi.org/10.1016/j.radonc.2021.03.017.

References

[1] Adelstein D, Gilliison, Pfister, Spencer S, Darlow SDJJotNCCNJ. NCCN guideline insights: head and neck cancers, Version 2.2017. 2017;15(6):761-70.
[2] Ferlay J, Soerjomataram I, Dikshit R, Eser S, Mathers C, Rebelo M, et al. Cancer incidence and mortality worldwide: sources, methods and major patterns in GLOBOCAN 2012. Int J Cancer 2015;136:E359–86.
[3] Steel GG, McMillan TJ, Peacock JH. The 5Rs of radiobiology. Int J Radiat Biol 1989;56:1045–8.
[4] Boustani J, Grapin M, Laurent PA, Apetoh L, Mirjolet C. The 6th R of radiobiology: reactivation of anti-tumor immune response. Cancers 2019;11.
[5] Kim HS, Kim SC, Kim SJ, Park CH, Jeung HC, Kim YB, et al. Identification of a radiosensitivity signature using integrative metaanalysis of published microarray data for NCI-60 cancer cells. BMC Genomics 2012;13:348.
[6] Eschrich SA, Pramana J, Zhang H, Zhao H, Boulware D, Lee JH, et al. A gene expression model of intrinsic tumor radiosensitivity: prediction of response and prognosis after chemoradiation. Int J Radiat Oncol Biol Phys 2009;75:489–96.
[7] Speers C, Zhao S, Liu M, Bartelink H, Pierce LJ, Feng FY. Development and Validation of a Novel Radiosensitivity Signature in Human Breast Cancer. Clin Cancer Res 2015;21:3667–77.
[8] Li G, Jiang Y, Lyu X, Cai Y, Zhang M, Li G, et al. Gene signatures based on therapy responsiveness provide guidance for combined radiotherapy and chemotherapy for lower grade glioma. J Cell Mol Med 2020;24:4726–35.
[9] Ji Y, Jiang Q, Jian G, Sun H, Wang Y, Qin H, et al. Developing a radiosensitivity gene signature for Caucasian patients with breast cancer. Oncol Rep 2018. https://doi.org/10.3892/or10.3892/or.2018.6567.
[10] Eschrich SA, Fulp WJ, Pawitan Y, Foekens JA, Smid M, Martens JWM, et al. Validation of a radiosensitivity molecular signature in breast cancer. Clin Cancer Res 2012;18:5134–43.
[11] Ahmed KA, Fulp WJ, Berglund AE, Hoffe SE, Dilling TJ, Eschrich SA, et al. Differences between colon cancer primaries and metastases using a molecular assay for tumor radiation sensitivity suggest implications for potential oligometastatic SBRT patient selection. Int J Radiat Oncol Biol Phys 2015;92:837–42.
[12] Ahmed KA, Chinnaiyan P, Fulp WJ, Eschrich S, Torres-Roca JF, Caudell JJ. The radiosensitivity index predicts for overall survival in glioblastoma. Oncotarget 2015;6:34414–22.
[13] Torres-Roca JF, Fulp WJ, Caudell JJ, Servant N, Bollet MA, van de Vijver M, et al. Integration of a radiosensitivity molecular signature into the assessment of local recurrence risk in breast cancer. Int J Radiat Oncol Biol Phys 2015;93:631–8.
[14] Strom T, Hoffe SE, Fulp W, Frakes J, Coppola D, Springett GM, et al. Radiosensitivity index predicts for survival with adjuvant radiation in resectable pancreatic cancer. Radiother Oncol 2015;117:159–64.
[15] Mohammadi H, Prince A, Figura NB, Peacock JS, Fernandez DC, Montejo ME, et al. Using the radiosensitivity index (RSI) to predict pelvic failure in endometrial cancer treated with adjuvant radiation therapy. Int J Radiat Oncol Biol Phys 2020;106:496–502.
[16] Eschrich S, Zhang H, Zhao H, Boulware D, Lee JH, Bloom G, et al. Systems biology modeling of the radiation sensitivity network: a biomarker discovery platform. Int J Radiat Oncol Biol Phys 2009;75:497–505.
[17] Scott JG, Berglund A, Schell MJ, Mihaylov I, Fulp WJ, Yue B, et al. A genome-based model for adjusting radiotherapy dose (GARD): a retrospective, cohort-based study. Lancet Oncol 2017;18:202–11.
[18] Jaffee EM, Dang CV, Agus DB, Alexander BM, Anderson KC, Ashworth A, et al. Future cancer research priorities in the USA: a Lancet Oncology Commission. Lancet Oncol 2017;18:e653–706.
[19] Poortmans P, Kaidar-Person O, Span P. Radiation oncology enters the era of individualised medicine. Lancet Oncol 2017;18:159–60.
[20] Masoudi-Khoram N, Abdolmaleki P, Hosseinkhan N, Nikoofar A, Mowla SJ, Monfared H, et al. Differential miRNAs expression pattern of irradiated breast cancer cell lines is correlated with radiation sensitivity. Sci Rep 2020;10.
[21] Li K, Zhu X, Li L, Ning R, Liang Z, Zeng F, et al. Identification of non-invasive biomarkers for predicting the radiosensitivity of nasopharyngeal carcinoma from serum microRNAs. Sci Rep 2020;10.
[22] Liu N, Boohaker RJ, Jiang C, Boohaker JR, Xu B. A radiosensitivity MiRNA signature validated by the TCGA database for head and neck squamous cell carcinomas. Oncotarget 2015;6:34649–57.
[23] Lin W, Huang Z, Xu Y, Chen X, Chen T, Ye Y, et al. A three-lncRNA signature predicts clinical outcomes in low-grade glioma patients after radiotherapy. Aging (Albany NY) 2020;12:9188–204.
[24] Wang Q, Fan H, Liu Y, Yin Z, Cai H, Liu J, et al. Curcumin enhances the radiosensitivity in nasopharyngeal carcinoma cells involving the reversal of differentially expressed long non-coding RNAs. Int J Oncol. 2014;44(3): 858-64.
[25] Stegle O, Teichmann SA, Marioni JC. Computational and analytical challenges in single-cell transcriptomics. Nat Rev Genet 2015;16:133–45.
[26] Ziegenhain C, Vieth B, Parekh S, Reinius B, Guillaumet-Adkins A, Smets M, et al. Comparative analysis of single-Cell RNA sequencing methods. Mol Cell 2017;65:631–643.e4.
[27] Onuchic V, Hartmaier RJ, Boone DN, Samuels ML, Patel RY, White WM, et al. Epigenomic deconvolution of breast tumors reveals metabolic coupling between constituent cell types. Cell Rep 2016;17:2075–86.
[28] Dong M, Thennavan A, Urrutia E, Li Y, Perou CM, Zou F, et al. SCDC: bulk gene expression deconvolution by multiple single-cell RNA sequencing references. Brief Bioinform 2020.
[29] Wang X, Park J, Susztak K, Zhang NR, Li M. Bulk tissue cell type deconvolution with multi-subject single-cell expression reference. Nat Commun 2019;10:380.
[30] Newman AM, Steen CB, Liu CL, Gentles AJ, Chaudhuri AA, Scherer F, et al. Determining cell type abundance and expression from bulk tissues with digital cytometry. Nat Biotechnol 2019;37:773–82.

[31] Puram SV, Tirosh I, Parikh AS, Patel AP, Yizhak K, Gillespie S, et al. Single-cell transcriptomic analysis of primary and metastatic tumor ecosystems in head and neck cancer. Cell 2017;171:1611–1624.e24.
[32] Lyu X, Zhang M, Li G, Jiang Y, Qiao Q. PD-1 and PD-L1 expression predicts radiosensitivity and clinical outcomes in head and neck cancer and is associated with HPV infection. J Cancer 2019;10:937–48.
[33] Langfelder P, Horvath S. WGCNA: an R package for weighted correlation network analysis. BMC Bioinf 2008;9:559.
[34] Panja S, Hayati S, Epsi NJ, Parrott JS, Mitrofanova A. Integrative (epi) genomic analysis to predict response to androgen-deprivation therapy in prostate cancer. EBioMedicine 2018;31:110–21.
[35] Liu J, Lichtenberg T, Hoadley KA, Poisson LM, Lazar AJ, Cherniack AD, et al. An Integrated TCGA pan-cancer clinical data resource to drive high-quality survival outcome analytics. Cell 2018;173.
[36] Ayers M, Lunceford J, Nebozhyn M, Murphy E, Loboda A, Kaufman DR, et al. IFN-γ-related mRNA profile predicts clinical response to PD-1 blockade. J Clin Invest. 2017;127(8):2930-40.
[37] Wilkerson MD, Hayes DN. ConsensusClusterPlus: a class discovery tool with confidence assessments and item tracking. Bioinformatics (Oxford, England) 2010;26:1572–3.
[38] Jiang P, Gu S, Pan D, Fu J, Sahu A, Hu X, et al. Signatures of T cell dysfunction and exclusion predict cancer immunotherapy response. Nat Med 2018;24:1550–8.
[39] Comprehensive genomic characterization of head and neck squamous cell carcinomas. Nature. 2015;517(7536):576-82.
[40] Carter SL, Cibulskis K, Helman E, McKenna A, Shen H, Zack T, et al. Absolute quantification of somatic DNA alterations in human cancer. Nat Biotechnol 2012;30:413–21.
[41] Wang Y, Wang R, Zhang S, Song S, Jiang C, Han G, et al. iTALK: an R Package to Characterize and Illustrate Intercellular Communication2019.
[42] Anderson AC. Tim-3, a negative regulator of anti-tumor immunity. Curr Opin Immunol 2012;24:213–6.
[43] Fourcade J, Sun Z, Pagliano O, Chauvin J-M, Sander C, Janjic B, et al. PD-1 and Tim-3 regulate the expansion of tumor antigen-specific CD8$^+$ T cells induced by melanoma vaccines. Cancer Res 2014;74:1045–55.
[44] Sakuishi K, Apetoh L, Sullivan JM, Blazar BR, Kuchroo VK, Anderson AC. Targeting Tim-3 and PD-1 pathways to reverse T cell exhaustion and restore anti-tumor immunity. J Exp Med 2010;207:2187–94.
[45] Ngiow SF, von Scheidt B, Akiba H, Yagita H, Teng MWL, Smyth MJ. Anti-TIM3 antibody promotes T cell IFN-γ-mediated antitumor immunity and suppresses established tumors. Cancer Res 2011;71:3540–51.
[46] Zhou Q, Munger ME, Veenstra RG, Weigel BJ, Hirashima M, Munn DH, et al. Coexpression of Tim-3 and PD-1 identifies a CD8+ T-cell exhaustion phenotype in mice with disseminated acute myelogenous leukemia. Blood. 2011;117 (17):4501-10.
[47] Liu J, Zhang S, Hu Y, Yang Z, Li J, Liu X, et al. Targeting PD-1 and Tim-3 pathways to reverse CD8 T-cell exhaustion and enhance ex vivo T-cell responses to autologous dendritic/tumor vaccines. J Immunotherapy (Hagerstown, Md : 1997). 2016;39(4):171-80.
[48] Kim JE, Patel MA, Mangraviti A, Kim ES, Theodros D, Velarde E, et al. Combination therapy with anti-PD-1, anti-TIM-3, and focal radiation results in regression of murine gliomas. Clin Cancer Res 2017;23:124–36.
[49] Watanabe N, Gavrieli M, Sedy JR, Yang J, Fallarino F, Loftin SK, et al. BTLA is a lymphocyte inhibitory receptor with similarities to CTLA-4 and PD-1. Nat Immunol 2003;4:670–9.
[50] Spodzieja M, Kuncewicz K, Sieradzan A, Karczyńska A, Iwaszkiewicz J, Cesson V, et al. Disulfide-linked peptides for blocking BTLA/HVEM binding. Int J Mol Sci 2020;21.
[51] Cristescu R, Mogg R, Ayers M, Albright A, Murphy E, Yearley J, et al. Pan-tumor genomic biomarkers for PD-1 checkpoint blockade-based immunotherapy. Science (New York, NY) 2018;362.
[52] Han H, Cho JW, Lee S, Yun A, Kim H, Bae D, et al. TRRUST v2: an expanded reference database of human and mouse transcriptional regulatory interactions. Nucleic Acids Res. 2018;46(D1):D380-d6.
[53] Foy JP, Bazire L, Ortiz-Cuaran S, Deneuve S, Kielbassa J, Thomas E, et al. A 13-gene expression-based radioresistance score highlights the heterogeneity in the response to radiation therapy across HPV-negative HNSCC molecular subtypes. BMC Med 2017;15:165.
[54] Wolf Y, Anderson AC, Kuchroo VK. TIM3 comes of age as an inhibitory receptor. Nat Rev Immunol 2020;20:173–85.
[55] Zeng J, See AP, Phallen J, Jackson CM, Belcaid Z, Ruzevick J, et al. Anti-PD-1 blockade and stereotactic radiation produce long-term survival in mice with intracranial gliomas. Int J Radiat Oncol Biol Phys 2013;86:343–9.
[56] Deng L, Liang H, Burnette B, Beckett M, Darga T, Weichselbaum RR, et al. Irradiation and anti-PD-L1 treatment synergistically promote antitumor immunity in mice. J Clin Invest 2014;124:687–95.
[57] Oweida A, Hararah MK, Phan A, Binder D, Bhatia S, Lennon S, et al. Resistance to radiotherapy and PD-L1 blockade is mediated by TIM-3 upregulation and regulatory T-cell infiltration. Clin Cancer Res 2018;24:5368–80.